Observing proposal for a LBT Large Program

The "PEPSI/LBT Exoplanet Transit Survey (PETS)"

P.I.: Klaus G. Strassmeier (AIP; kstrassmeier@aip.de; +49-331-7499-223)

Co-I(s): Christian Veillet (LBTO), Ilya Ilyin (AIP), Ji Wang (OSU), Scott Gaudi (OSU), Evgenya Shkolnik (ASU), Jennifer Patience (UoA), Everett Schlawin (UoA), Daniela Sicilia (INAF), Lorenzo Pino (INAF), Luca Malavolta (INAF), Alessandro Sozzetti (INAF), Aldo Bonomo (INAF), Francesco Borsa (INAF), Gaetano Scandariato (INAF), Valerio Nascimbeni (INAF), Karan Molaverdikhani (LSW), Thomas Henning (MPIA), Fei Yan (MPIA), Katja Poppenhäger (AIP), Matthias Mallonn (AIP), Engin Keles (AIP).

Summary of observing request for this project: total of 593 hrs distributed in 2021AB, 2022AB, and 2023AB.

Doc revision history

Issue	Date	Changes	Responsible
V0.1	18.7.2020	Initial draft	kgs
V0.2	27.7.2020	First in-house distribution	kgs
V0.3	12.8.2020	First target update. Distributed to all.	kgs
V0.4	…	Version for first zoom	kgs
V0.5	22.8.2020	Feedback from first zoom included	kgs
V0.6	15.9.2020	New target suggestions included/revised	kgs
V0.7	18.9.2020	Dates and Times revisited	kgs
V0.8	25.9.2020	Added results from Workshop	kgs
V1	30.09.2020	Submitted version	
V1.1	18.12.2020	Targets in Table T1 updated/corrected	kgs

About this document

This document is a proposal for an exoplanet transit survey with LBT and PEPSI. It describes the survey, its scientific aims and goals, the observing plan, the targets, the deliverables, and the management structure.

Abbreviations

PEPSI	Potsdam Echelle Polarimetric and Spectroscopic Instrument
LBTO	Large Binocular Telescope Observatory
CD	Cross Disperser
TESS	Transiting Exoplanet Survey Satellite
SDS	Spectroscopic Data Reduction software package for PEPSI (SDS4PEPSI)
DR	Data reduction
RV	Radial velocity
FITS	Flexible Image Transport System
PFU	Permanent Fiber Unit
DSP	Deep Spectrum Project
KSP	Key Science Project
AGw	Acquisition, Guiding, and Wavefront sensing units
SAN	Storage Area Network
MAST	Mikulski Archive for Space Telescope
HJ	Hot Jupiter
UHJ	Ultra-hot Jupiter
IRT	Infrared triplet (of Ca II)
VLT	ESO Very Large Telescope
HST	Hubble Space Telescope
GTC	Gran Telescopio Canarias

Contents

1. Executive summary

We propose a high-resolution spectroscopic survey of exoplanet transits, secondary eclipses, and host-star characterizations of a total of 29 targets. Immediate goal is to characterize their planetary atmospheres in detail. While transit data allow the extraction of the planetary spectrum at the terminator through transmission at high atmospheric altitudes giving insights on atmospheric chemical species and atmospheric dynamics, the eclipse data allow tracing atmospheric emission from lower altitudes on the dayside of the exoplanet (c/o Fig. 1). The strengths and uniqueness of this proposal are the combination of PEPSI's spectral resolution and throughput and the light-collecting power of the LBT in binocular mode with a concerted consideration of the applicable science cases. An additional bonus is the possibility of a dual use of high and low resolution instruments like PEPSI and MODS as well as the detailed characterization of the host star from the co-added time-series spectra allowing, for example, relating Fe/H ratios in planetary atmospheres to those in stellar atmospheres. Moreover, flexible scheduling of the observations will be possible because PEPSI is on stand-by all the time and is useable in remote control. A typical use case is monitoring a transit in two wavelength regions (two PEPSI cross dispersers) at R=130,000 and then re-observing the target for the superior conjunction phases shortly before and after planet eclipse, depending on the science case. Although this proposal is dedicated to the detailed characterization of exoplanet atmospheres, some unique targets with starspots or circumplanetary material are proposed to be monitored for science related to stellar activity and star-planet relations as well. The survey requests 59.3 nights in total, or 15 nights per semester, for three years in order to observe a representative number of targets. Key instrumental numbers like, for example, the resolution × wavelength coverage × S/N product are otherwise only matched by the VLT and *Espresso* in the southern hemisphere.

2. Science cases

Determining the nature and diversity of planetary atmospheres is a key objective of exoplanet science. It is our primary aim. The characterization of such atmospheres is the path to understand whether planets of our solar system, and in particular Earth-like planets in the future, are the exception or the standard in our Universe. It is likely the key science for the next generation of extremely large telescopes and should lead to the detection of bio-signatures and eventually of life. Thanks to their large atmosphere, the spectroscopic observation of hot (HJ) and ultra-hot (UHJ) Jupiters (that is Jupiter type planets which orbit their host star in very close orbits) allows us to test our interpretative tools already now but also to investigate the formation and evolution of exoplanetary systems. A secondary aim of this survey is to determine and relate planetary atmospheric parameters to precise stellar parameters like chemical surface abundances, in particular for some of the new planet-host stars from the NASA TESS mission (Ricker et al. 2014, SPIE **9143**). Stellar host characteristics are important to be known to a good accuracy in order to describe and understand the planets discovered. The following Fig. 1, borrowed from van Boekel et al. (2012, SPIE **8442**, 1) and based upon Seager & Deming (2010, ARA&A **48**, 631), visualizes an exoplanet eclipse geometry like we will use in this proposal.

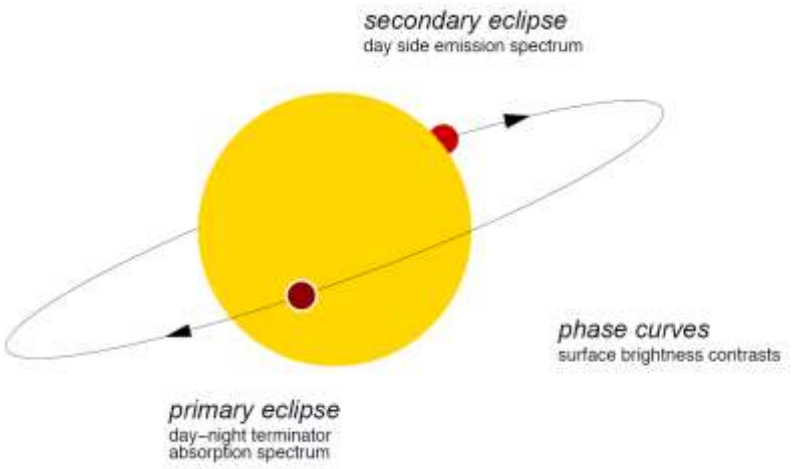

Fig. 1. The eclipse depth in primary eclipse (=planet transit) is the fraction of stellar light blocked by the planet. It shows minute wavelength-dependent variations if the high planetary atmospheric layers contain spectroscopically active chemical species. In secondary eclipse (=planet occultation) we observe light coming from the planet's day side. At optical wavelengths this is typically dominated by stellar photons scattered by the planet atmosphere or reflected off the surface, while in the infrared we see the planet's thermal emission. The thermal emission spectra as a function of orbital phase, or for non-transiting systems, are currently not part of this proposal. Figure from van Boekel et al. (2012, SPIE **8442**, 1).

One of the central aims of our survey is the characterization of a statistically significant amount of exoplanets, and to put the findings into a bigger context. For this, one immediate goal is the detection of atmospheric line absorbers like Fe I using CD II (426-480nm) and/or III (480-544nm) in PEPSI's blue arm, or like the alkali elements sodium and potassium or the singly-ionized calcium infrared triplet in PEPSI's red arm. It will enable us, for example, to infer the Fe/H content on these planets. Comparing this and other ratios to the host star's chemical abundances will constrain the formation and evolution of these planets in a wider context and helps to probe planetary winds and possible depletion processes in their atmospheres (e.g., Yan et al. 2020, A&A **640**, L5; Wang et al. 2020, AJ **160**, 150). H_2O, CH_4, and HCN are bio-relevant molecules and can be studied at longer wavelengths with CD VI (742-910nm) in the red arm, albeit extremely weak. C_2H_2, C_2H_4, C_2H_6 are also relevant photochemical haze precursors. These can be investigated for planets with moderate temperatures (T_{eq}<1000 K) at no additional cost if CD VI is chosen for a transit/eclipse but, like for the other molecules, detections remain at best difficult.

Almost all targets proposed in this survey have more than one science case, which allows for more than one team to work on the same transit/eclipse data. As an example, PEPSI's three red-arm CDs can be used to investigate preferentially alkali lines and molecular lines to determine the evaporation of planetary atmospheres, stratospheric dynamics and the existence of inversion layers, or the planet's rotation, while the blue-arm CDs can be used to study preferentially metal lines. While there are challenges, for example in measuring the inversion layer of HJs and pinning down the species that are responsible for the inversion layer, high resolution spectroscopy in the optical wavelengths with 8-10m telescopes/instruments can meet these challenges. This makes each individual target essential for this proposal and in sum has the merit of low risk.

Finally, LBT is among the few 8-10m observatories in the world that practically allows for simultaneous multi-instrument multi-resolution observations, which greatly benefit the removal and mitigation of instrumental and/or astrophysical systematics (e.g., PEPSI+MODS simultaneous high-resolution and low-resolution optical observation).

What follows is a summary of the science cases for our proposed PEPSI/LBT exoplanet transit survey.

2.1 Detection and Statistics of Stratospheres in Atmospheres of Hot Jupiters

The stratosphere is a layer of the atmosphere where the temperature increases with altitude. Our Earth has a stratosphere because ozone absorbs energy from incoming ultraviolet radiation from the Sun. While theories predict that TiO and VO molecules may serve as a radiation absorbent to cause a stratosphere in a hot Jupiter, definitive detection of TiO/VO has been made for only one HJ. Only at sufficiently high equilibrium temperatures does TiO/VO appear (similar to the transition between L and M dwarfs) and contribute to the opacity that causes stratospheres. The transition temperature is thought to be around 2000 K (Fortney et al. 2008, ApJ **678**, 1419). Despite great effort, it is still unknown whether a stratosphere is a rare or a common phenomenon in exoplanets. We propose to survey for TiO and address the frequency of stratospheres in HJs. The result will provide crucial constraints on input parameters (e.g., pressure-temperature profile) in modeling exoplanet atmospheres. Recent studies predict that the cause for the temperature inversion could be induced by Fe I rather than TiO, where Fe I emission lines are found on WASP-189b (Yan et al. 2020, A&A **640**, L5), on WASP-33b (Nugroho et al., 2020, ApJ **898**, L31), WASP-121b (Gibson et al., (2020, MNRAS, in press) and KELT-9b (Pino et al. 2020, ApJ **894**, L27). However, using CD III of PEPSI, Fe I lines could be inferred and using CD V TiO could be inferred, thus the investigation of both absorber species would be possible (see also Sect. 2.4).

Nugroho et al. (2017, AJ **154**, 221) detected TiO in WASP-33b at very high spectral resolution (R=165,000). Their method involved cross-correlating a TiO template with observed spectra. This template matching method exploits spectral diversities such as radial velocity (RV) and chemical composition: the RV of the planet follows its orbital motion and TiO only exists in planetary atmosphere. A spectrograph with high spectral resolution can be more effective in discerning planet RV and resolving planet TiO lines. In the optical region, the resonant doublets of sodium and potassium have large absorption cross sections, hence, a larger absorption in the transmitted signal of these lines is expected in HJs. Resolving the core of the alkali lines with high-resolution spectroscopy, will allow to retrieve the temperature-pressure profile and to understand if the planet is evaporating or not. Moreover, a Doppler-shift of these features could indicate the presence of winds while a kinematic broadening could trace a super-rotation at high altitudes, that is a rapid large-scale circulation of atoms in the upper layers of the atmosphere (Seidel et al. 2019, A&A **623**, 166).

We simulate a case in which an UHJ is observed simultaneously by PEPSI (R=130,000, 628-742 nm) and MODS (R=2000, 600-900 nm). Simulated data are generated by petitRADTRANS (Mollière et al. 2019, A&A **627**, A67); a few predicted spectra for a series of atomic and molecular transitions are shown in Fig. 2. Typical uncertainties are assumed: 2500 ppm per spectral channel for MODS and a peak-to-peak 0.5% fluctuation of planet absorption spectra extracted form PEPSI data. There are multiple parameters that we attempt to retrieve including surface gravity, cloud deck pressure (also a good approximation for the H^- opacity), and opacity. For TiO and VO, the simulation shows that the joint PEPSI+MODS analyses returns a more constraining retrieval result because the loss of continuum information in high-resolution data, which causes the correlation between TiO and VO abundance, is recovered in the low-resolution data. We plan for a few targets with visits in the dual PEPSI+MODS configuration in this survey.

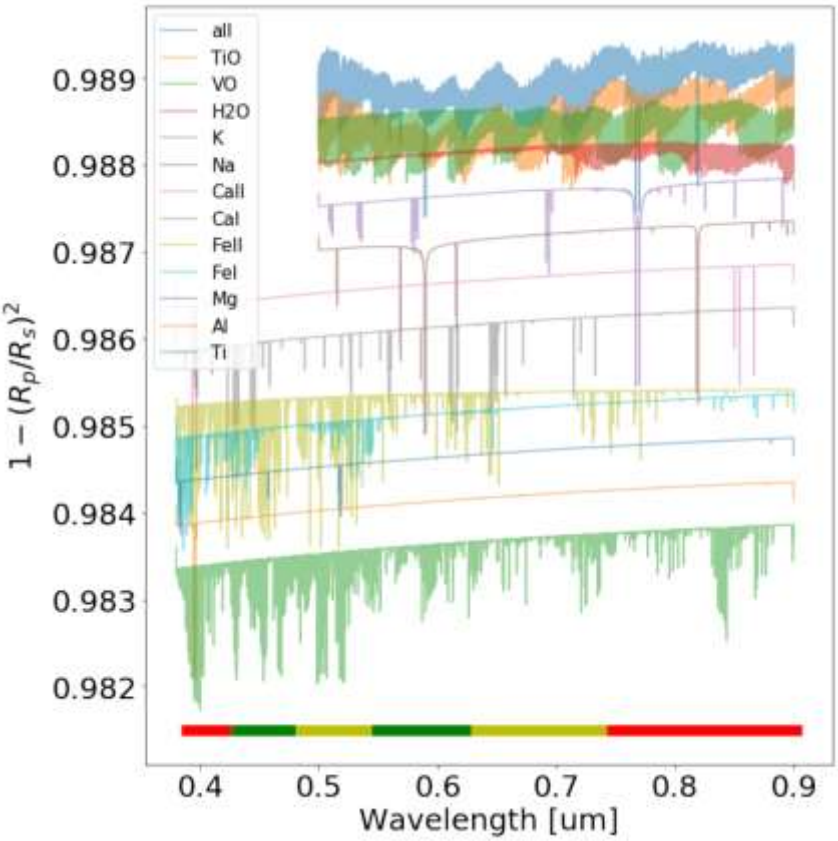

Fig. 2. Transmission spectrum template for a variety of atomic and molecular species. The spectra are generated by petitRADTRANS. PEPSI wavelength coverage is indicated by the color bar at the bottom. The same color means these wavelength ranges can be simultaneously observed.

2.2 Velocity Dynamics in the Atmospheres of Ultra-Hot Jupiters

Transiting planets with very short orbital periods have strong atmospheric dynamics that can be probed via transmission spectroscopy. However, there is little empirical understanding of hot planet rotation periods, wind speeds, and atmospheric expansion velocities. Promising candidates need to be observed at very high signal-to-noise in order to disentangle the various contributions from the shape of atomic transmission spectra and advance our understanding of the dynamics in these extreme planet atmospheres. We will utilize the excited hydrogen transitions Hα and Hβ and search for absorption from neutral magnesium, for which we made the first detection in an exoplanet atmosphere with PEPSI in 2018B (KELT-9b; Cauley et al. 2019, AJ **157**, 69; Fig. 3). Just recently, we re-observed the transmission spectrum of the hot gas giant WASP-33b with LBT/PEPSI in order to further constraint its atmospheric dynamics and mass loss rate (Cauley et al. 2020, ApJ, in press). WASP-33b is an excellent transmission spectroscopy target and it is one of the hottest transiting planets discovered to date (Collier Cameron et al. 2010, MNRAS **407**, 50). WASP-33 is also relatively bright (V = 8.1mag), and has a large transit depth (≈1.1%) and low-density atmosphere. Besides, its planet has been the focus of a few transmission spectroscopy studies, with reported detections of aluminum oxide (von Essen et al. 2019, A&A **622**, 71) and titanium oxide (Nugroho et al. 2017, AJ

154, 221). It is also a good candidate for the detection of Mg I (Johnson et al. 2015, ApJ **810**, L23, Watanabe et al. 2020, PASJ **72,** 19). As a secondary science product, our proposed transit would add another epoch to a nodal precession analysis.

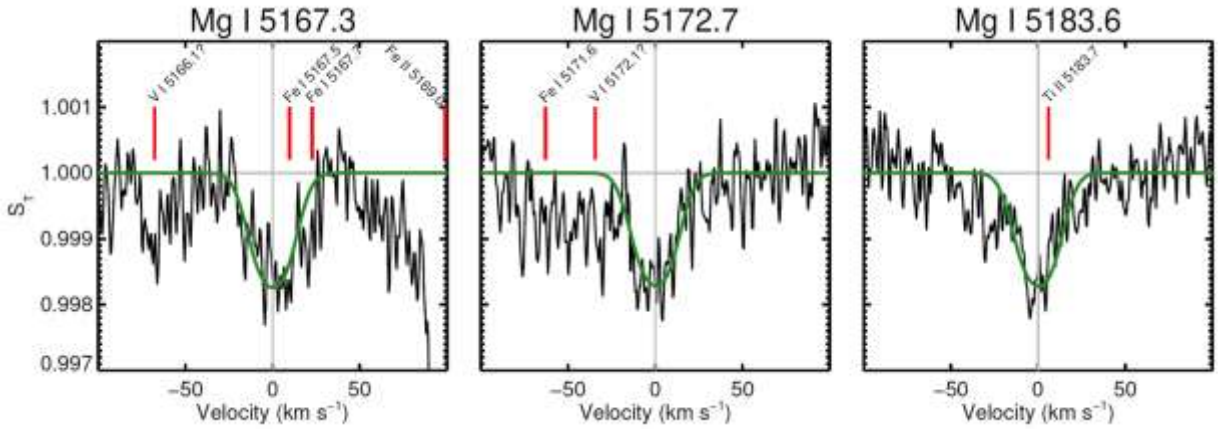

Fig. 3. Average line profiles for the Mg I triplet lines of the KELT-9 b atmosphere from PEPSI/LBT. S_T is the ratio stellar spectrum in transit divided by the stellar spectrum out of transit. Possible contaminating atomic transitions are marked with vertical red lines. Spectral resolution R is 50,000. From Cauley et al. (2019, AJ **157**, 69).

Our most recent PEPSI observations of WASP-33b revealed Hα and Hβ absorption centroids consistent with a rotational velocity of its thermosphere of 10 km/s (Cauley et al. 2020, ApJ, in press). We also measured a strong blue-shift in the average in-transit spectrum which is naturally explained by a global wind across the planet's terminator. Planets around A-stars with very short orbital periods, that is *P*(orb) approximately ≤5 days, are subject to tremendous amounts of stellar radiation. The atmospheric dynamics of such hot gas giants are extreme, with wind speeds reaching many kilometers per second in the thermosphere and day-to-night side flows of a few kilometers per second. The outflow velocities of escaping material can reach approximately 10 km/s as the result of thermal expansion. Atmospheric dynamics may even provide information on planetary magnetic field strengths due to the influence of magnetic fields on the velocity and outflow structure. It may be possible to investigate the magnetic field on exoplanets directly: Helling et al. (in prep.) suggest that measuring metallic ion/neutral abundances and their Doppler shifts could separate two scenarios for ionospheric morphology: day-tonight vs. zonal winds. A zonal wind scenario is suggestive of an ionosphere at the photospheric levels and a possibly strong magnetic field. Understanding the atmospheric physics of these objects is thus the next step towards a more complete characterization of exoplanets. We now can apply the WASP-33b models to the other targets in this survey that have detectable transmission spectrum absorption (i.e., KELT-9b, KELT-20b, HD 189733b).

2.3 Detecting Metals in the Atmospheres of Ultra Hot Jupiters

Planetary atmospheres contain a wealth of diagnostic information on basic planetary conditions like climate and composition, with the latter being a diagnostic of planetary formation conditions. Most atmospheric characterization of abundances and temperature profiles has been driven by low resolution space-based transit spectroscopy. A novel ground-based approach that leverages high spectral resolution cross-correlation spectroscopy has been steadily gaining in its utility and reliability for atmospheric characterization. We propose to perform high spectral resolution time series cross-correlation spectroscopy on, e.g., WASP-189b. WASP-189b is among a sparsely populated class of intriguing UHJs (T_{eq} > 2600K) and is one of the best targets amenable to high-resolution cross-correlation emission spectroscopy, a state-of-the-art technique for measuring atmospheric properties from the ground. A first attempt with PEPSI and the LBT had resulted in no consistent atmospheric absorption beyond the 1-2σ level (Cauley et al. 2020, arXiv 2004.06859, RNAAS) but a revisit is highly desirable. UHJs are unique in that they are presumed to have physics/chemistry similar to those of late M-dwarf photospheres, and also at these temperatures condensates rarely play a role and thus should allow for a “clean” measurement of the composition, enabling precise determinations of

fundamental quantities like the metallicity, and carbon-to-oxygen ratio in the infrared. The spectroscopic presence of numerous metal species (e.g., Fe, Ti, Mg) emission features, the lack of obscuring condensates on the planetary dayside, and favorable planet-to-star flux ratios make UHJs ideal targets for precision metallicity detections (Hoeijmakers et al. 2018, Nature **560**, 453). We also propose PEPSI transmission spectroscopy of WASP-76b (R_p = 1.83 R_J; M_p = 0.92 M_J), one of the hottest known exoplanets (T_{eq} ≈2200 K). Just recently, Ehrenreich et al. (2020, Nature, **580**, 597) used the new *Espresso* spectrograph at the VLT to measure the velocity centroids of Fe I absorption in the atmosphere of WASP-76b.

We also note that cloud formation might occur even on UHJ's night-side, which is likely affecting the morning limb as well. Such cloud formation results in C/O enhancement (Helling et al. 2019, A&A **626**, A133**;** Molaverdikhani et al. 2020, ApJ **899**, 53). Therefore, the observed C/O, and possibly any other elemental abundance ratios, is not equivalent to the bulk elemental abundance ratios. But we have the tools to investigate their connection and interpret their bulk elemental abundances.

An extra bonus for targets with detected metals is provided by the atmospheric Rossiter-McLaughlin (RM) effect.
The atmospheric RM effect is a deviation of the in-transit RVs from the classical RM effect that happens when the atmosphere of the planet is intercepted by the mask used to create the stellar cross-correlation functions. This effect was first discovered for KELT-9b (Borsa et al. 2019, A&A **631**, A34), and later confirmed with the analysis of other two UHJs (Borsa et al., Rainer et al., priv. commun.). By analyzing the shape of the RV deviation, we can measure the extension of the planetary atmosphere that correlates with the stellar mask. This means basically that we can measure the amount of Fe I in the planetary atmosphere only by studying the calculated stellar RVs. This technique can be applied for UHJs with Fe I in their atmospheres.

2.4 Day-side Spectra of Exoplanets around the Secondary Eclipses

Just recently, Nugroho et al. (2020, ApJ **898**, L31) detected Fe I emission on the day-side of WASP-33b at the 6.4-σ level from high-resolution spectra taken with the 8.2-m Subaru telescope. This confirmed the existence of a thermal inversion on the day-side of the planet which is very likely to be caused by the presence of neutral iron and previously-detected TiO (see also Yan et al. 2020, A&A **640**, L5 for WASP-189b, or Pino et al. 2020, ApJ **894**, L27 for KELT-9b). While the classical transit data (=primary eclipse) allow the extraction of the planetary spectrum at the terminator through transmission at high atmospheric altitudes, the secondary eclipse data allow tracing atmospheric emission from lower altitudes on the dayside of the exoplanet. Our approach in this survey is including the secondary eclipse for a number of our targets with reasonable expectation for such detection (e.g. for HD80653b, HAT-P70b, or WASP-43b). These targets are identified in Sect. 4. Note that the science cases have different priorities from target to target (but see Sect. 2.1 for the general case). From our experience we state that using the data during the secondary eclipse as a stellar master spectrum does not improve the analysis. It would also require as much telescope time as the observations of the planet day-side itself. So we attempt not to observe the phases during secondary eclipses but only shortly before and shortly after the eclipse.

2.5 Evaporating Atmospheres: the Effect of near-UV Radiation on Hydrodynamic Escape of Hydrogen

One important aspect affecting exoplanets is the stellar environment. In this work, we aim to investigate the evaporation of exoplanet atmospheres driven by the host star near- UV radiation. For this, we aim to observe the absorption at the Balmer-lines during the exoplanet transit of KELT-17b and KELT-18b. Modeling approaches predicted that massive exoplanets are stable to catastrophic atmospheric escape. We aim to study the triggering of atmospheric escape induced by near-UV stellar irradiation by probing the upper and middle atmospheres of exoplanets with short orbital distances. For UHJs, the hydrogen Balmer lines enable constraining the temperature-pressure profile of the planetary atmosphere in the region subject to strong heating and therefore constrain the energetics driving the escape (Fossati et al. 2020, A&A, submitted).

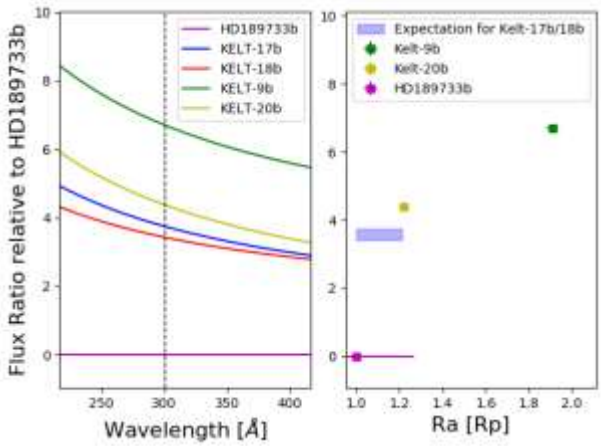

Fig. 4. Near-UV flux ratio relative to HD189733b (log-scale) for different exoplanets (left) and their probed atmospheric radius at ~300 nm (right).

We compare the Hα absorption on three HJs being HD189733b (Cauley et al. 2017, AJ **153**, 217), KELT-20b (Casasayas-Barris et al. 2019, A&A **628**, A9) and KELT-9b (Cauley et al. 2019, AJ **157**, 69) to our targets of interest. For illustration purposes, Fig. 4 shows (left) the near-UV flux which each of the exoplanets receives from its host star relative to the one which HD189733b receives (log-scale). The same is compared to those Hα absorption levels (at 300 nm, dashed line in the left panel) in units of the atmospheric radius which is probed (right). Comparing both figures, one can see that the detected Hα absorption increases with the increase in near-UV radiation that the exoplanets receive. We aim to put our survey targets of interest, KELT-17b and KELT-18b, into this bigger context. To derive the Hα absorption on both planets the "excess method" or the "division method" are suitable, which are common techniques to derive atmospheric absorption (see, e.g., Redfield et al. 2008, ApJ **673**, L87; Yan & Henning, 2018, Nature Astr. **2**, 714).

2.6 Spin-Orbit Alignment and Metal Content of the Atmospheres of Super-Neptunes and Sub-Saturns

The origin of low-mass planets ($M < 0.3$ M_J) in a strongly irradiated environment involves interaction with the host star radiation and likely migration, but still escapes our understanding. Nevertheless, both phenomena impact the planet atmospheres and spin-orbit alignment. We will observe two transits for each selected object to measure, firstly, their spin-orbit alignment through the RM effect and, secondly, the thermal and dynamical conditions in their upper atmosphere under the effect of strong irradiation through the resonant sodium and potassium doublets. We expect that the collecting power of LBT will provide the highest significance detection of alkali doublets to date in this class of planets, allowing us to probe the outermost, thin layers of the gas escaping the planets' atmospheres.

Spin-orbit misalignment. The orbital inclination gives useful information to constrain the possible migration history of a planet (e.g., Bourrier et al., 2018, Nature **533**, 477). The magnitude of the RM effect scales with the planet size, and is thus challenging to measure it for Neptune-sized planets. Indeed, the alignment angle has only been measured for four super-Neptunes (3 misaligned, 1 aligned). Thanks to the large LBT collecting area, we will use PEPSI to measure the effect for the planets that we selected, adding importantly to the existing sample.

Metal content. The Na I absorption signature (Huitson et al., 2012, MNRAS **422**, 2477) is a powerful probe of the temperature and pressure profile of exoplanets (Heng et al. 2015, ApJ **803**, L9; Pino et al. 2018, A&A **619**, A3). High spectral resolution observations can constrain atmospheric properties up to the base of the thermosphere, where the heating responsible for photo-evaporation takes place (Murray-Clay et al., 2009, ApJ **693**, 23), sounding the thermal structure, winds and super-rotation throughout the upper atmosphere of the planets.

2.7 Doppler Tomographic Measurement of Spin-Orbit Misalignments and Nodal Precession

Time-series spectra through exoplanet transits also allow us to measure the alignment (or lack thereof) of the planetary orbit with respect to the stellar spin using the Rossiter-McLaughlin effect (and, indeed, accurately modeling the RM signature in the spectra is required for the transmission spectroscopy analysis). As a planet transits a rotating star, light from the obscured stellar surface elements does not contribute to the formation of the rotationally-broadened line profile, causing a perturbation to the line profile at velocities corresponding to those of the obscured surface elements. This perturbation can either be detected directly (Doppler tomographic analysis), or as an anomalous radial velocity shift during transit due to the changing line centroid (radial velocity RM analysis). The spin-orbit misalignment is a tracer of a planet's dynamical history and origins (e.g., Winn & Fabrycky 2015, ARA&A **53**, 409). Chromatic RM can be used to infer the broadband transmission spectrum too, as the amplitude of RM is directly related to the planetary radius (Di Gloria et al. 2015, A&A **580, A84;** Oshagh et al. 2020, submitted). Furthermore, the spin-orbit misalignment and/or impact parameter can change over time due to nodal precession of the planetary orbit; detection of this effect produces unique constraints on the stellar interior structure. We will perform these analyses for all of our targets, but the spin-orbit misalignment measurements will be most useful for previously-unobserved TESS discoveries. We expect to be able to detect or constrain the precession rate for Kepler-13Ab (Masuda 2015, ApJ **805**, 28), KELT-9b (Ahlers et al. 2020, AJ **160**, 4), and perhaps MASCARA-1b for the first time, and more precisely measure the precession rate of WASP-33b (Watanabe et al. 2020, PASJ **72**, 19). We show a previous PEPSI Doppler tomographic dataset from Johnson et al. (2018, AJ **155**, 100) in Fig. 5 below.

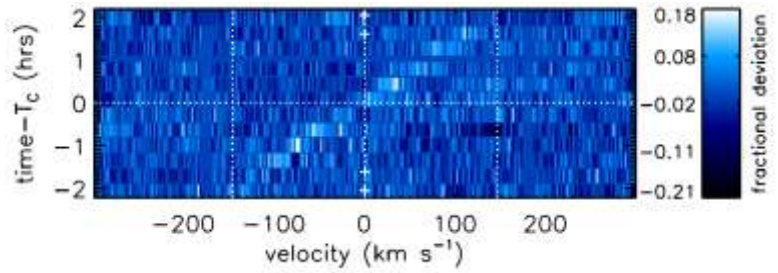

Fig. 5. Doppler tomographic observation of KELT-21b from LBT/PEPSI in 2017A (Johnson et al. 2018, AJ **155**, 100). Each colorscale row shows the deviation in the line profile from the out-of-transit line profile; time increases from bottom to top. The line profile perturbation due to the transiting planet is the bright streak moving from lower left to upper right.

2.8 Depletion of Alkali Metals in Giant Planet Atmospheres

Exoplanet atmospheres show great diversity triggered by the difference in planetary radius, mass and equilibrium temperature, which affects the atmospheric chemistry. Using high resolution spectroscopy, atomic absorption at low pressure level can be determined and compared for different exoplanets. The aim of this project is to investigate on-going atmospheric depletion processes in “hotter” and “colder” hot Jupiter atmospheres by exploring the atmospheric Na and K absorption features, which are one of the opaquest sources in the optical wavelength range. Applying high resolution spectroscopy, Na has been detected on several exoplanets, e.g., HD189733b (Wyttenbach et al. 2015, A&A **577**, A62), WASP-49b (Wyttenbach et al. 2017, A&A **602**, A36), on Wasp-76b (Seidel et al. 2019, A&A **623**, A161), on WASP-52b (Chen et al. 2020, A&A **635**, A171) and many more, whereas K has been detected only on HD189733b (Keles et al. 2019, MNRAS **489**, L37) and WASP-52b (Chen et al. 2020, A&A **635**, A171) in high resolution observations. In general, both alkalis have similar condensation and photo-ionization properties and should show similar absorption properties. However, Keles et al. (2020, MNRAS **498**, 1023) showed that the difference in the absorption line profiles of these alkalis can be used to probe the planetary winds and possible depletion processes in such atmospheres. We aim to observe the alkalis on different tempered Jupiter type planets that receive different stellar radiation and to put the ongoing alkali line absorption and depletion into a bigger context. As mentioned above, high-res alkali (and in particular Na) lines can be obscured by clouds/haze. This additional information imprinted in these lines could be used to study the pressure levels and opacities of these particles (Khalafinejhad 2020, in prep.). This can be done for all planets with available low-resolution spectra in the optical.

Specifically, we aim to compare alkali metal absorption with previously acquired PEPSI data of HD189733b and HD209458b (representing the “colder” targets with lower equilibrium temperature). A newly-discovered planet

offers the opportunity to perform such a measurement and combine it with Hα. V1298 Tau b is a transiting warm Jupiter discovered by David et al. (2019, ApJ **885**, L12) using data from the Kepler extended mission K2. We propose to also observe this young warm Jupiter V1298 Tau b, but note that its ephemeris must be refined before we can reliably schedule it in 2022.

2.9 Detecting Exospheric Emission on Rocky-Exoplanets

The characterization of the atmospheres of extrasolar planets plays an important role in our understanding of the planetary origin and evolution. A suitable method is to analyze transmitted light from the atmosphere of an exoplanet, as it can reveal fingerprints of atoms and molecules. Our aim is to detect exospheric Na I D and Ca II IRT emission from the transiting planet 55 Cnc e, orbiting a K-star with an apparent magnitude of *V*=5.95 mag. The exoplanet 55 Cnc e is the biggest close-in (~18hr orbit) terrestrial exoplanet (~8 Earth-masses) around such a bright star, which makes it the most favorable target for investigation on atmospheric loss processes, induced by intense stellar radiation. Other possible targets for this are HD219134b and c (=GJ892), which orbit a 5.6-mag early K-type star (Tanner et al. 2010, PASP **122**, 1195; Ligi et al. 2019, A&A **631**, A92). The strength of the exospheric Ca II and Na I emission will allow for estimations of these loss processes, revealing information about the planet's surface composition. Up to now, there is no significant detection of atmospheric constituents of rocky-exoplanets, thus possible first evidence would have a high impact on the investigation of future terrestrial exoplanets.

Ridden-Harper et al. (2016, A&A **593**, A129) made a first attempt to observe the exosphere of 55 Cnc e, by investigating on the Na and Ca II H&K lines, combining different HARPS, HARPS-N and UVES observations. The results showed a 3σ and 4.1σ detection for Ca II and Na respectively. However, due to the large uncertainties of the observations, the authors did not claim detection. Instead, they supported an estimation of 0.0023 sodium and 0.07 Ca II signal relative to the stellar flux. Angelo & Hu (2017, AJ **154**, 232) investigated thermal emission properties of the super-Earth exoplanet 55 Cnc e using Spitzer phase curves, stating a possible atmosphere with an atmospheric pressure of ~1.4 bar. Esteves et al. (2017, AJ **153**, 268) searched for water absorption in high resolution spectra applying the cross-correlation method, stating the evidence for a water rich atmosphere with a volume mixing ratio > 10%, however, being in tension with Jindal et al. (2020, AJ **160**, 101) and Bourrier et al. (2018, A&A **619**, A1) predicting a water-poor atmosphere as the atmosphere is strongly irradiated. We expect a strong water feature in WASP-76b because of its low surface gravity and hot equilibrium temperature (Stevenson 2016, ApJ **817**, L16). In general, water has been repeatedly observed in the atmospheres of other HJs both from space with HST/WFC3 and from the ground at high resolution in the NIR, and both in absorption (e.g., Evans et al. 2016, ApJ **822**, L4) and in emission (Birkby 2013, MNRAS **436**, 35).

2.10 Probing Atmospheres of Super-Earths

Exploring the atmosphere of super-Earths is the next step toward characterization of earth-like atmospheres in the future. A sample of nearby super-Earths over different equilibrium temperatures provides the first statistical insight on their composition and their evolution.

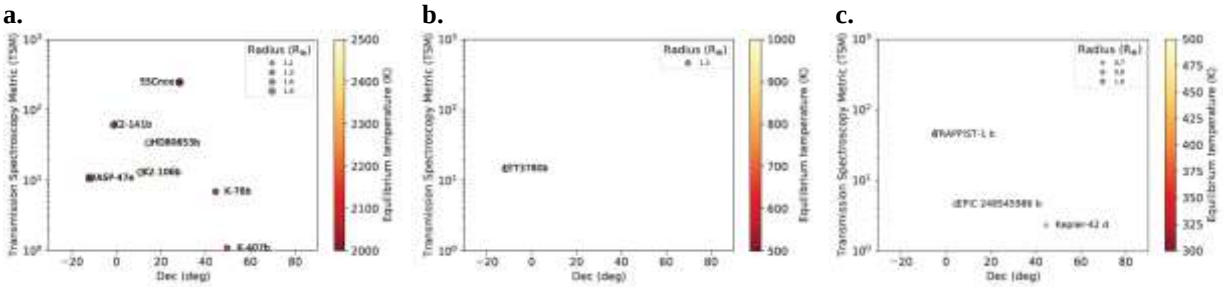

Fig. 6 Transmission Spectroscopy Metrics (TSM; y-axis) vs. declination (x-axis) for some Super-Earths. From left to right: **a.** the hottest known small super-Earths (R<2.0R⊕) and RV>35 km/s, **b.**, the known small super-Earths with T_{eq}<1000 K and RV>10 km/s and, **c.**, the known small super-Earths with T_{eq}<500 K and RV of a few km/s (all for the date of writing).

Ultra-hot super-Earths (Teq > 2000 K): They are the best candidates to study super-Earths' exospheres and possible surface compositions. The Transmission Spectroscopy Metric (TSM) of the hottest known small super-Earths (R<2.0$R_\oplus$) with high radial velocity during transit (RV>35km/s) are shown in Fig. 6a. High radial velocity during the transit and high TSM are the keys to increase the chance of atmosphere detection on small planets. HD 80653 b is the hottest among these planets and the best candidate (Frustagli et al. 2020, A&A **633**, A133), as proposed for this case study.

Hot super-Earths (Teq < 1000 K): Photochemical haze production is expected to enhance at temperatures below 1000 K (Gao et al. 2020, Nature Astr., submitted). In addition, water and methane production is expected to dominate over CO and H_2 production at these temperatures (e.g., Molaverdikhani et al. 2019, ApJ **873**, 32; ApJ **883**, 194; Molaverdikhani et al. 2020, ApJ **899**, 53). Hence, characteristic of atmospheres over these temperatures are expected to be significantly different from that of hotter planets. Fig. 6b is similar to Fig. 6a except for planets with T_{eq}<1000 K and radial velocity during transit of more than 10 km/s. The only accessible candidate is LTT 3780 b. This planetary system is a recent TESS discovery with two planets on the opposite sides of the radius gap, which makes this system also to be the best-known system to investigate the radius gap. Both planets have high TSM and are suitable for transmission spectroscopy (Nowak et al. 2020, A&A, arXiv:2003.01140). However, these observations remain high risk (but also high gain).

Warm super-Earths (Teq < 500 K): Fig. 6c is again similar to Fig. 6a except for planets with T_{eq} < 500 K and radial velocity during transit of more than a few km/s. TRAPPIST-1 b is the best candidate (Gillon et al. 2016, Nature **533,** 221), given its high TSM. There have been some atmospheric studies of this system but no *high resolution atmospheric characterization* has been published yet. Low-resolution studies have not discovered molecular features and this can be further investigated using PEPSI. The star is on the faint end of what PEPSI can reach but still accessible (Strassmeier et al. 2018, SPIE **10702**, 12). A review of possible planetary atmospheres in the TRAPPIST-1 system was recently published by Turbet et al. (2020, SSRv **216**, 100), summarizing that these planets are "likely to have either (i) a high molecular weight atmosphere or (ii) no atmosphere at all." Given the fact that there has been no published work on high-resolution ground-based observations of this system, they conclude that "near-infrared high-resolution ground-based spectrographs on existing very large and forthcoming extremely large telescopes will bring significant advances". LBT's light-collecting power may still be not enough but can help to address this question, while this won't be achievable by 4m telescopes at all. Again, this set of targets is high risk, and high gain.

2.11 Water and Potassium on the Exoplanet HAT-P-1b: a Show Case for LBT Binocular Capability

The presence and detection of water especially in HJ systems can be used to estimate the relative abundance of this species and estimate the carbon-to-oxygen ratio, which gives clues about the formation and migration history of these planets (see, e.g., Öberg et al. 2011, ApJ **743**, L16). Furthermore, the intensity of the water bands indicates if an additional source of opacity such as clouds or hazes is present in the atmosphere (e.g., Pont et al. 2013, MNRAS **432**, 2917; Sing et al. 2016, Nature **529**, 59). The aim is to confirm the presence of water in the optical wavelength range 730 nm to 910 nm as well as the detection of atomic potassium at 769 nm in the atmosphere of HAT-P-1b from high-resolution spectra. Wakeford et al. (2013, MNRAS **435**, 3481) already presented a transmission spectrum of HAT-P-1b based on one transit observation between 1.1 μm and 1.7 μm using the HST. Wilson et al. (2015, MNRAS **450**, 192) showed a potassium detection using narrow-band photometry with GTC-Osiris with a mean 5.1σ detection. However, Todorov et al. (2019, A&A **631**, A169) investigated the Na-absorption using low resolution data and stated a non-detection. HAT-P-1b would be the first planet that would possess K rather than Na, making the investigation of the potassium feature in high resolution very important.

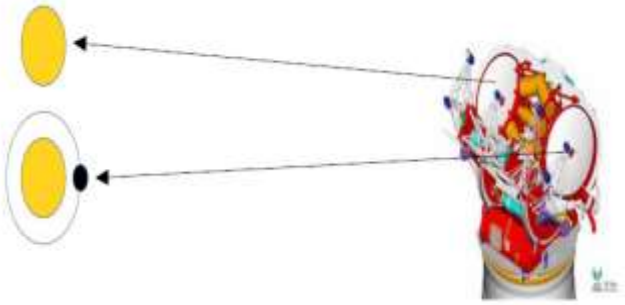

Fig. 7. Schematic setup for the transit observations of HAT-P-1b. This target belongs to a close visual binary system with components 11" apart and of similar physical properties and characteristics of which one has a planet. The use of PEPSI and LBT provides the possibility to observe independently and simultaneously the component with the transiting planet and the other component as a reference star.

The present proposal employs the unique capability of having two telescopes feeding one spectrograph; thus presents a new idea for investigating atmospheric atoms and molecules in wavelength regimes where many telluric lines usually hamper their detection. The host-star is the binary HAT-P-1. This star belongs to a visual binary system with components that exhibit similar physical properties and characteristics and are 11" apart. The use of the LBT in dual monocular mode (c/o Fig. 7) provides the possibility to observe the transiting planet and a reference star independently and simultaneously. The collected spectra are expected to have identical telluric fingerprints and are therefore suitable to solve the telluric contamination problem. The binary system HAT-P-1 = ADS 16402 consist of two main-sequence stars (a G0-type and a F9-type star) where both stars have V-magnitudes of 10.4. The hot Jupiter HAT-P-1b (R_p~1.3R_J) orbits the slightly cooler G-type star. For each star, after calibrating the spectra to the same wavelength, a mean spectrum of the (expected) 25 exposures will be produced and each exposure divided by the mean spectrum. This gives for both targets a residual telluric spectrum without stellar lines for each exposure. The difference between both targets will be that one star will have a planetary signal included whereas the other one will not. Due to the fact that both stars with similar magnitude are exposed at the same time at nearly identical S/N, the telluric residual spectra will be identical as well.

The resonant (neutral) K-line at 7664Å is usually not accessible in high resolution observations due to the strong telluric oxygen absorption. The simultaneous observation of both stars will deliver a perfect telluric template and will make this K-line accessible, as well as the planetary water absorption in the visible wavelength range (applying cross-correlation technique) which are usually strongly blended by telluric water lines. Because the transit lasts for up to 7 hrs, we propose alternating the red-arm CDs between CD IV (sodium) and CD VI (potassium).

2.12 Testing the Solar Activity Paradigm with Starspots

Transits of exoplanets across cool stars contain blended information about structures on the stellar surface and about the planetary body and atmosphere. The discovery of transiting exoplanets has opened up a new way of studying stellar surface structures: the transiting exoplanet acts as an occulting disk moving across the features within the transit path. This fairly novel way to achieve high-resolution information for stellar surface structures along the transit path is of critical importance to studying exoplanetary atmospheres through transit spectroscopy (e.g., Seager & Sasselov 2000, ApJ **537**, 916): the light passing through the exoplanetary atmosphere contains information about the atmospheric structure, but to extract it unambiguously, the properties of the light source need to be known. That light source is the photospheric patch that lies behind the exoplanetary atmosphere in the line-of-sight towards the observer, as discussed in detail by, e.g., Rackham et al. (2018, ApJ **853**, 122; 2019, AJ **157**, 96). This presents a challenge and opportunity combined: the emission properties of the stellar surface structures along the transit trajectory as well as the transmission properties of the exoplanetary atmosphere can be analyzed in a joint study of the spectrum that carries information on both source and absorber (see Schrijver 2020, ApJ **890**, 121). In this way we may extract spatially-resolved spot parameters like size and shape as well as higher-layer atmospheric parameters above the spot, including metallicity and other abundance ratios if detected. We propose observing the spotted host-star HAT-P-11 during a transit of its planet b (Morris et al. 2017, ApJ **846**, 99) but in POL mode. This shall enable the first direct detection of the magnetic field of a starspot (for indirect detections see the review by Strassmeier 2009, A&ARv **17**, 251).

2.13 Characterizing the Host Stars

The chemical composition of a planet-hosting star is known to influence the architecture of its planetary system (e.g., Dawson & Murray-Clay 2013, ApJ **767**, L24; Adibekyan et al. 2013, A&A **560**, A51). Statistical surveys of exoplanet host stars show that Jupiter-like giants are preferentially formed around metal-rich stars (Fischer & Valenti 2005, ApJ **622**, 1102; Udry & Santos 2007, ARA&A **45**, 397), while smaller planets appear to be less selective (e.g., Buchhave et al. 2014, Nature **509**, 593). This has been interpreted as evidence for the prevalence of the core accretion model of planet formation (Ida & Lin 2004, ApJ **616**, 567; Mordasini et al. 2009, A&A **501**, 1161). However, work by Nayakshin (2017, PASA **34**, 2) has shown that formation by gravitational instability via the tidal downsizing model can also reproduce the observed correlation between giant planets and host star metallicity. On the other hand, the formation of terrestrial planets does not seem to prefer iron-rich environments and succeeds with similar frequency around stars of various metallicities. Nevertheless, recent studies have hinted at some chemical preference for terrestrial planets. In particular, Adibekyan et al. (2015, A&A **581**, L2) showed that metal-poor planet hosts tend to have a higher [Mg/Si] ratio than metal-poor stars without detected planets.

The secondary goal in this survey is to use the transit time-series spectra also for a detailed chemical characterization of the host stars. Whenever needed, further observations in other wavelength regions are planned. The proposed targets are identified and marked in Tables T1-T4 in Sect. 5. These observations are gap fillers and are not explicitly scheduled as a separate visit but are carried out whenever the weather pattern and the transit start/end allow. This gives enough flexibility to react in case unexpected bad weather occurs during an ongoing transit/eclipse run. There is one exception; one out of the 58 nights is dedicated to the characterization of V1298 Tau (proposed GTO night of 12.12.2022). It is a B=11.1-mag K2 dwarf star and we expect an integration time of 1 hr for S/N≈100 in the blue CD I. Four such exposures are required for S/N≈200, which is the minimum S/N for a good chemical analysis in the wavelength region 383-410nm.

3. Deliverables

3.1 PEPSI instrumental boundary conditions for this survey

In its PFU mode PEPSI is available with three spectral resolutions, *R*, averaging 50,000, 130,000, and 250,000 over the 385-915nm wavelength range. The default pixel sampling is now two pixels per resolution element for all resolutions. A high-sampling mode for *R*=50,000 with 12 pixels, and for *R*=130,000 with 4 pixels, is still available on demand. Fiber sky apertures for the three resolutions are 2.3", 1.5", and 0.74", respectively. Under good weather conditions with seeing of 1" and moderate air mass, a 10-min integration of a 10.0-mag G2 star yields a S/N per pixel of 520/370 for CD V/III at *R*=50,000, 250/170 at *R*=130,000, and 80/55 at *R*=250,000. Thus, a practical brightness limit for exoplanet transits appears to be around V=15th magnitude at *R*=50,000 in 20-min exposures when a S/N per pixel of 60 is achieved in the most efficient CD-V. Radial velocity (RV) stability is independent of the observing mode but resolution, stellar spectral morphology, intrinsic line broadening, and S/N limit the RV precision to ≈1 m/s over a few hours of a transit and not better than ≈5 m/s over an observing semester. Science cases that require very precise RVs will be conducted with the sky-fibers carrying light from the Fabry-Perot etalon. Its integration time is automated and linked to the total target integration time. Otherwise, the sky fibers will carry usual sky light (from a position approximately 6" off the target position).

3.2 Anticipated data product

The data product is a time series of spectra in two wavelength regions for, depending on the science case, the planet transit and the planet eclipse, and even other orbital phases. It is mandatory in any case to additionally cover the target for up to one hour prior and one hour after the transit/eclipse in order to get a sufficient number of out-of-eclipse spectra for appropriate comparison.

We chose the following wavelengths as our most-wanted CD-combinations for the blue and the red arm respectively:

1. CD-III (480-544nm) and CD-V (628-741nm).
2. CD-III (480-544nm) and CD-VI (742-910nm).
3. CD-II (426-480nm) and CD-IV (544-628nm).

Figure 8 shows the data product based on a previous example of an individual *R*=130,000 spectrum. Figure 9 shows four selections of interesting line regions from this example. The choice of the appropriate CD is science-case and transit-duration dependent. Changing a CD in either arm takes only about one minute and one could aim for alternating CDs during a transit series if the time and the sampling requirements allow. With CD-IV we would have access to the sodium D lines but with CD-VI to the Ca infrared triplet (IRT) and the two potassium lines (lithium is included in CD-V). The two PEPSI dichroids do not allow using CD-IV when the adjacent CD-III disperser is in the blue beam, so IV and III cannot be used simultaneously. CD-III for a second visit has the appeal of increasing the S/N if needed and keeping the possibility for a direct comparison of certain line profiles as a function of time, e.g., for Hβ but also the Mg I triplet around 5170 Å. Another option is to observe a second transit for a subset of interesting targets and then get enhanced wavelength coverage including, for example sodium. This remains an option and depends on the prioritized science case per target.

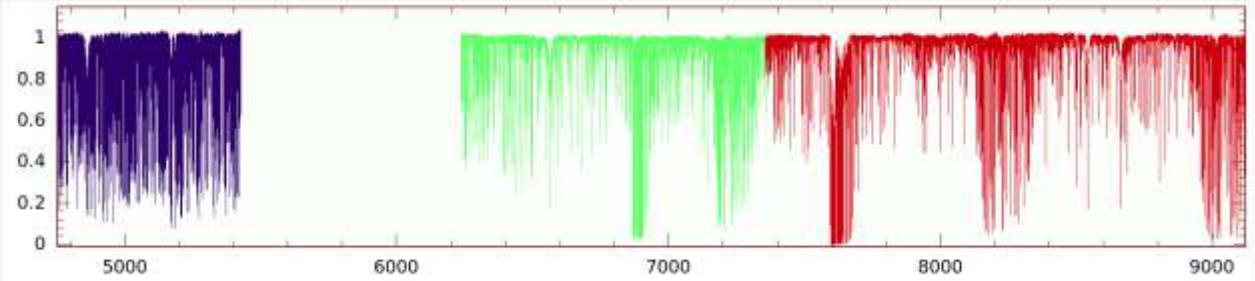

Fig. 8. Example spectrum of the wavelength coverage for cross dispersers CD-III, CD-V and CD-VI (from left to right color coded). The blank region is otherwise covered by CD-IV. Resolution is 130,000.

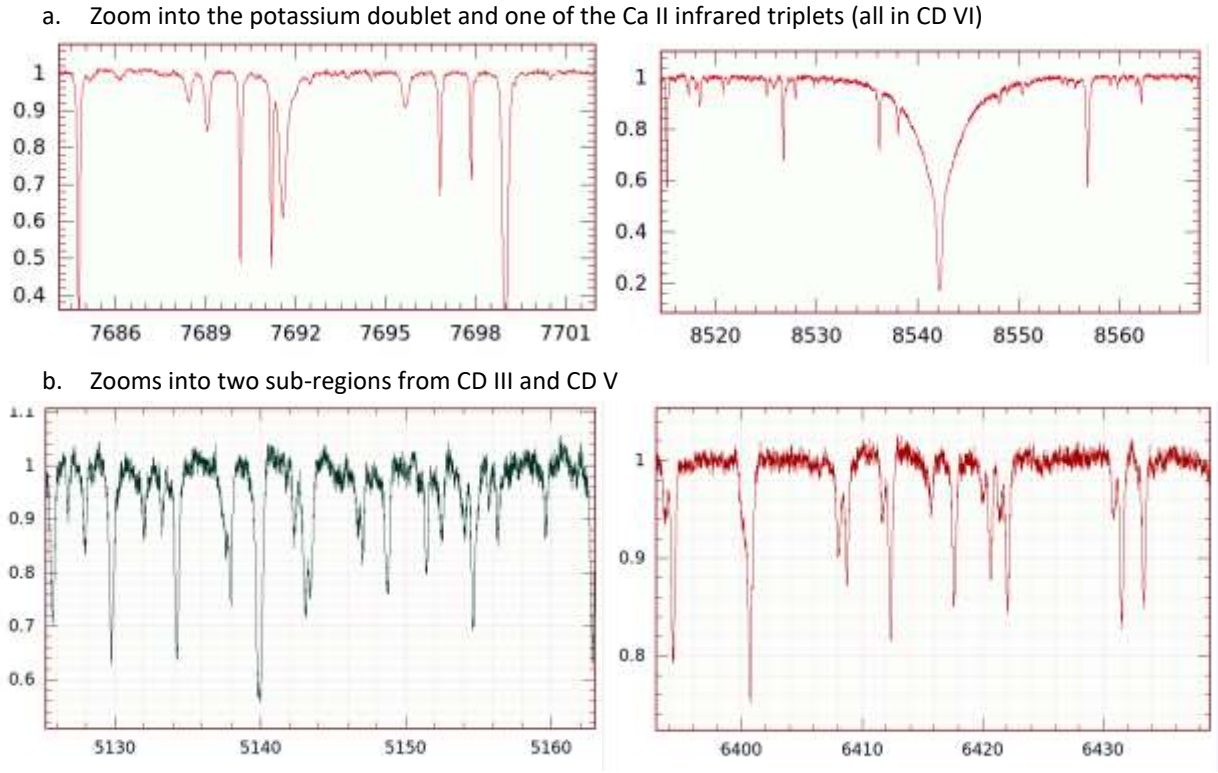

Fig. 9. **a.** Two zooms into sub-regions from CD-VI (left: potassium; right Ca II IRT line). S/N is 250:1 in this example, which is the expected S/N for a 10th mag star and a 10-min integration. **b.** Two zooms into sub-regions of ≈40 Å. S/N ratio is 70:1 in CD III (left) and 155:1 in CD V (right) in this example.

Transit spectrum example. We obtained PEPSI data for KELT-20b in May 2019. The extracted planet line profile immediately shows the blue-shift that is expected from the day-to-night wind for HJs. We measured a blue-shift value of -2.2±0.2 km/s with respect to the planet rest frame. This is consistent with the previously reported values of -2.4±1.0 km/s (Casasayas-Barris et al. 2019, A&A **628**, A9). We note that our single line (Fe II 5018 Å; Fig. 10 below) has a higher S/N than that from HARPS-N. This is because PEPSI provided 14 data points sampling the line whereas there are only 3 data points for the HARPS-N data, and each data point has a comparable uncertainty. It showcases the light collecting power of the dual-aperture LBT, which allows us to complete tasks such as conducting spatially-resolved wind speed measurement.

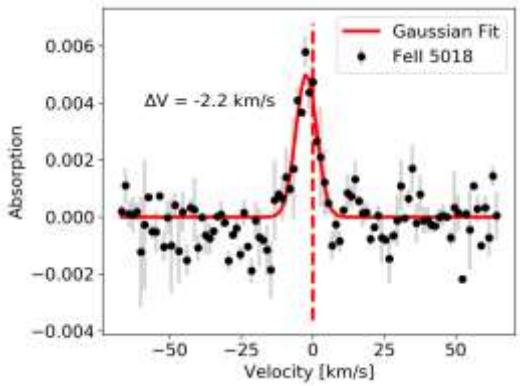

Fig. 10. Line profile of Fe II 5018 Å from KELT-20 b observed with PEPSI in 2019. The integrated velocity of this line is blueshifted by 2.2±0.2 km/s, consistent with predictions. From Ji Wang, OSU, priv. commun..

4. Target list

4.1 Transit merit of already characterized targets

We used the exoplanet library https://exoplanet.eu for a first target selection based on transit parameters. A transit merit function is computed constrained by a period P<10 d, brightness V<11 mag, and planet's radius R_{planet} > 0.8 $R_{Jupiter}$ for a R=130,000 integration of 10 min. Table 1 lists the 39 highest merit targets meeting above criteria. Obviously, there is not a shortage of targets.

Table 1. Transit ranking based on P < 10 d, V < 11 mag, and R_{planet} > 0.8 $R_{Jupiter}$ (with a few exceptions). Column SNR is the expected S/N ratio per pixel; Rp planet radius; Teq equilibrium temperature of the planet; Mp planet mass; Rs stellar radius; Vmag V-magnitude of host star; TSM transit merit normalized to first entry.

Rank	Planet	SNR	Rp	Teq	Mp	Rs	Vmag	TSM
(1,	'WASP-127	', 96,	1.37,	1400.0,	0.18,	1.39,	10.1,	1.0)
(2,	'WASP-181	', 119,	1.184,	1186.0,	0.299,	0.965,	10.0,	0.8458289511521414)
(3,	'HAT-P-47	', 106,	1.313,	1605.0,	0.206,	1.515,	10.6,	0.8180284015213212)
(4,	'WASP-033	', 306,	1.679,	2710.0,	2.16,	1.509,	8.3,	0.8007202319279267)
(5,	'WASP-069	', 109,	1.057,	963.0,	0.26,	0.813,	9.87,	0.727292616049191)
(6,	'WASP-076	', 141,	1.854,	2228.0,	0.894,	1.765,	9.5,	0.720615891058809)
(7,	'KELT-20	', 426,	1.735,	2261.0,	3.52,	1.561,	7.58,	0.5889008532613286)
(8,	'KELT-07	', 274,	1.533,	2048.0,	1.28,	1.732,	8.54,	0.5282534295812977)
(9,	'HAT-P-01	', 116,	1.319,	1322.0,	0.525,	1.174,	10.4,	0.4893977834132097)
(10,	'55_Cnc_e	', 900,	0.169,	2349.0,	0.024,	0.954,	6.0,	0.4645211332977159)
(11,	'WASP-013	', 115,	1.528,	1531.0,	0.512,	1.657,	10.42,	0.4493884736810113)
(12,	'KELT-08	', 92,	1.86,	1675.0,	0.867,	1.67,	10.83,	0.41105851223642836)
(13,	'HAT-P-60	', 145,	1.631,	1772.0,	0.574,	2.197,	9.7,	0.40437368909241844)
(14,	'KELT-23	', 96,	1.322,	1561.0,	0.938,	0.995,	10.4,	0.3742026053412281)
(15,	'HAT-P-30	', 98,	1.34,	1630.0,	0.711,	1.215,	10.42,	0.3684244194791126)
(16,	'KELT-17	', 174,	1.525,	2087.0,	1.31,	1.645,	9.3,	0.3658121918011484)
(17,	'HD_332231	', 245,	0.867,	876.0,	0.244,	1.277,	8.56,	0.3534427465750851)
(18,	'WASP-074	', 128,	1.404,	1926.0,	0.826,	1.536,	9.7,	0.35259936411752524)
(19,	'WASP-189	', 494,	1.374,	2641.0,	2.13,	2.33,	6.6,	0.29352799114726685)
(20,	'WASP-012	', 63,	1.9,	2580.0,	1.47,	1.657,	11.7,	0.2812611905037548)
(21,	'K2-232	', 138,	1.08,	999.0,	0.408,	1.252,	9.8,	0.2738402165243549)
(22,	'HAT-P-17	', 105,	1.01,	792.0,	0.534,	0.838,	10.54,	0.22933062277787172)
(23,	'KELT-06	', 106,	1.193,	1313.0,	0.43,	1.58,	10.38,	0.2212751904877128)
(24,	'KELT-18	', 113,	1.57,	2085.0,	1.18,	1.908,	10.1,	0.214602527932304)
(25,	'HAT-P-06	', 109,	1.395,	1704.0,	1.063,	1.518,	10.5,	0.20655463231258053)
(26,	'HAT-P-13	', 101,	1.487,	1725.0,	0.906,	1.756,	10.62,	0.20622761818631935)
(27,	'XO-7	', 66,	1.373,	1743.0,	0.709,	1.48,	10.5,	0.19356465090777808)
(28,	'WASP-082	', 106,	1.712,	2202.0,	1.248,	2.219,	10.1,	0.19279057700493352)
(29,	'KELT-02	', 245,	1.29,	1712.0,	1.524,	1.836,	8.7,	0.17593190783908888)
(30,	'MASCARA-1	', 277,	1.5,	2570.0,	3.7,	2.1,	8.3,	0.14760323726892502)
(31,	'WASP-084	', 76,	0.976,	833.0,	0.687,	0.768,	10.83,	0.1464204288686125)
(32,	'HAT-P-70	', 159,	1.87,	2562.0,	6.78,	1.858,	9.5,	0.1143700016865223)
(33,	'EPIC_201498078	', 78,	0.84,	1066.0,	0.179,	1.669,	10.6,	0.09950427208355288)
(34,	'HAT-P-69	', 113,	1.626,	1990.0,	3.73,	1.854,	9.8,	0.0757353744904233)
(35,	'HD_118203	', 293,	1.133,	1496.0,	2.173,	2.103,	8.05,	0.06648927790614464)
(36,	'KELT-24	', 215,	1.272,	1458.0,	5.18,	1.506,	8.4,	0.05523972691369121)
(37,	'WASP-086	', 103,	0.632,	1415.0,	0.821,	1.291,	10.66,	0.0270335877369375)
(38,	'HAT-P-02	', 248,	1.19,	1516.0,	8.74,	1.68,	8.71,	0.025830310272439764)
(39,	'V1298_Tau_b	', 113,	0.904,	677.0,	2.2,	1.305,	10.1,	0.015251719904432727)

4.2 Northern TESS targets

These targets are not fully known at the time of writing of this proposal but are already in the TESS MAST pipeline. An update is given on their web page: https://tess.mit.edu/publications/. TESS is discovering planets at a fast and steady pace: approximately 180 planet candidates per month. Enormous effort is currently underway to conduct follow-up observations and confirm TESS planet candidates. While the current majority of TESS planet candidates are in the southern sky, TESS footprint is now covering also the northern sky with currently (08/2020) 10 confirmed planets with a declination above zero. There are more than 200 planets waiting to be confirmed in early 2020 (see Wang et al. 2013, ApJ **776**, 10 for the follow-up effort to exclude false positives). As of July 2020, TESS went into its 27 months long extended mission. During its last 15 months it will observe the northern hemisphere again (July 2021 to July 2022).

Possible TESS Targets in 2022 or 2023:
TOI-1899, NGTS-11, TOI-1728, HD332231, GJ357, LTT1445, TOI-197.

4.3 Benchmark Targets

We envision re-observing a number of targets with well-defined parameters and/or other interesting discoveries. We call these target benchmark targets as we will compare our PEPSI transits with their literature results and thereby gain a better insight into external errors.

The classics: **HD189733** and **HD209458**. These are among the best studied exoplanet systems to date and LBT/PEPSI had already contributed to its growing knowledge (Keles et al. 2019, MNRAS **489**, L37; 2020, MNRAS, in press). We aim to reobserve at least HD 189733b again.

Young exoplanets. These are interesting because their atmospheres are still evolving, plus they are expected to still be internally hot, therefore they will have a large and well observable scale height. Unfortunately, many of the rather near-by ones are from the first batch of TESS data, so they are on the southern sky. However, there is one bright enough exception (below), and more will be discovered in the next half year with the northern TESS data:

V1298 Tau. 25 Myr host star, 4 planets with the innermost having a period of around 8 days. All expected to be puffy. TESS transit depth of innermost one is ≈0.15%, but the thin atmosphere above should be really extended due to its youth. Star is not quite as bright as we would like it to be (V=10.1mag), but again there is the large expected scale height of the thinner atmosphere and the star is magnetically active, Hα is not really probing the escaping material; it forms at pressures in these atmospheres where the material is still gravitationally bound and is only moving at upward velocities of ~1 km/s.

Exoplanets around Hot Stars. These are interesting because they live in extreme optical and UV environments, and may be undergoing catastrophic UV-driven escape. This could be big, if true. There are quite a few targets now available in the north:

KELT-20 (Teff=8730K, 3.5 day period, 1.3% optical transit depth, V=7.6)
Kepler-13A (Teff=7650K, 1.8 day period, 0.8% optical transit depth, V=9.7)
KELT-17 (Teff=7454K, 3.1 day period, 0.9% transit depth, V=9.2)
WASP-33 (Teff=7430K, 1.2 day period, 1.1% transit depth, V=8.1)

Exoplanets in Binary Stars. Here we have one favorable case for a unique LBT binocular application.

HAT-P1;
Kepler-13A.

Rocky Planets. Here we also have two targets which had been scheduled already but lost due to bad weather. The other one is new.

55 Cnc e;
HD219134bc (=Gl892);
TRAPPIST-1b;
LTT3780b.

Neptune-sized Planets with spotted host star. The following is, so far, the best case.

HAT-P11;
V1298 Tau.

Spin-orbit misalignments. Depending on the data, likely all transit data can be searched for spin-orbit misalignment. Preference will be given to targets with highly inclined orbits. Among other possible targets are:

MASCARA-1;
Kepler-13A;
KELT-9;
WASP-33.

5. Telescope operations plan

5.1 Total telescope time needed

For making an impact in the current literature, we believe that a total of ≈30 targets is needed. The detailed determination of the requested telescope time is summarized below in Table 2. Its content is based on the targets and dates/times listed in Tables T1-T4 (their columns D are the actual transit/eclipse times). To the transit times we add one hour of out-of-transit observations before and one hour after the transit, in sum two hours per visit. Similarly is assumed for the eclipse times but then to cover the eclipse itself if visible ("star-without-planet spectra"). In case the host star shall be characterized according to Sect. 2.13, we add two one-hour integrations in the four CDs that were not requested for the transit/eclipse of that target. Additionally, for every visit, we add one hour of overhead time (to compensate for telescope collimating and initial target set-up). Note: exposures for host-star characterization are unscheduled in time but are planned as fill-ins when a transit/eclipse observation does not need the entire night, or a transit/eclipse target reaches too high an air mass, or a transit/eclipse had been interrupted due to clouds etc..

Table 2 summarizes our need for a total of 693 hours of telescope time (i.e., 69.3 nights w/ 10 hrs per night). It includes the bad-weather compensation for targets lost from the four one-quarter LBT partners. The PEPSI GTO time of 10 nights (identified as "GTO" in Tables T1-T4) is included in the number of total hours but is not eligible for bad-weather compensation. **Therefore, the total telescope time requested in this proposal is 593 hrs or 59.3 nights, and we thus ask on average for 15 nights from each one-quarter LBT partner over three years (3.7 nights per semester per quarter partner).**

The bad weather fail rate is assumed to be 50% (see also Sect. 5.5). Compensation is planned always one year later in the next A or B semester. After a successful mid-term evaluation of the survey, we propose to schedule those targets that failed due to bad weather in 2022AB. These should then be re-scheduled for 2023AB if their science case is still valid then. On average, this adds another 112 hours (28 hrs per ¼ partner) for 2023AB. Tables 3 and 4 are an attempt to show the partner distribution and compare the partner shares.

Table 2 - Summary of requested telescope time including bad-weather compensation.

	Transit time (hours)	Pre- and postransit (hours)	Host-star character. (hours)	Overhead (hours)	TOTAL (hours)
2021A	70	34	13	17	**134**
2021B	72.5	34	15	17	**138.5**
2022A[(a)]	50.5+32[(b)]	26+16[(b)]	9	13+8	**154.5**
2022B[(a)]	37+32[(b)]	22+16[(b)]	19	12+8	**146**
2023AB	64	32	8	16	**120**
SUM	358	180	63	91	**693**

Notes: (a) We assume 8 weathered-out targets from each of the previous semesters that then shall be re-observed in 2022AB and 2023AB. (b) Time estimated for the 8 targets per semester with "averaged" transits of 4hrs + 2hrs pre/post transit + 1hr overhead (the targets themselves are naturally not known now). The "Overhead" is set as 1hr per night for telescope collimating and initial target acquisition, and its failure handling.

Table 3 - Partner shares in hours (including targets from bad-weather compensation + overhead for 2021-22).

	Arizona	OSU/RC	INAF	LBTB	GTO
Transit/ eclipse	40.5	39	58.5	49	44
Pre- and post time	18	22	26	28	22
Host star	3	0	30	0	23
Bad-weather	56	56	56	56	0
Overhead	9	11	13	14	11
TOTAL	**126.5**	**128**	**183.5**	**147**	**100**

Notes: The assumed "bad-weather targets" are accounted for as additional time but cannot be specified for which partner. We assume it equally distributed among the partners (14 hrs per ¼ partner per semester) over two years. GTO is not eligible for bad-weather compensation and thus no GTO targets will be re-observed.

Table 4 - Time breakdown into institutional sub-partners per semester. Values are hours.

	Arizona	OSU/RC	INAF	LBTB
2021A	UoA 0.0 ASU 5.5	OSU 19.5	INAF 42.5	MPIA 33.0 AIP 5.0
2021B	UoA 0.0 ASU 8.0	OSU 14.0	INAF 23.0	MPIA 20.5 AIP 16.5
2022A	UoA 8.0 ASU 15.0	OSU 25.5	INAF 37.0	MPIA 0.0 AIP 8.0
2022B	UoA 20.5 ASU 13.5	OSU 13.0	INAF 25.0	MPIA 8.0 AIP 0.0
SUM	**UoA 28.5 ASU 42.0**	**OSU 72.0**	**INAF 127.5**	**MPIA 61.5 AIP 29.5**
Bad weather compensation	56	56	56	56
TOTAL	**126.5**	**128.0**	**183.5**	**147.0**

Notes: UoA University of Arizona; ASU Arizona State University; OSU Ohio State University; INAF Istituto Nazionale di Astrofisica; MPIA Max-Planck-Institute for Astronomy; AIP Leibniz-Institute for Astrophysics Potsdam.

5.2 Target schedule per semester

Tables T1 – T4 list the targets, the favored transit times, the favored eclipse times if desired, and flags if host-star characterization is desired. Alternative transit and eclipse dates are given (the "Prio" numbering in the tables reflects the priority assigned by the proposer). Column D specifies the transit time and duration in hours UT. We again emphasize that sufficient pre- and post-transit/eclipse time had been added, that is 1 hour before and 1 hour after transit and up to 2 hours during eclipse. The two columns *R* and CD specify the desired spectral resolution mode and the cross dispersers, respectively. Integration time is not specified at this time because it is usually 10 minutes except for the most bright stars (then 5 min) and the very faint stars (then 15-20min), but can also be defined alternatively as the desired S/N (PEPSI then chooses the integration time based on the exposure meter with a built-in maximum time). The "Program Principal Investigator" (PPI) is identified in column PPI. The last column labelled *Account*

identifies the accounting of the telescope time to the four ¼ LBT partners. For the time being, the programs are final for the first two semesters of observations. Semester 3 and 4 (year 2022) are preliminary and will then take into account the failed targets from semesters 1 and 2. Semester 5 and 6 (year 2023) contains only the failed targets from 2022. The following is the number of independent visits for the four semesters that shall be scheduled[1].

Run 2021A: 17 Visits on schedule (Table T1, p.22).

Run 2021B: 17 Visits on schedule (Table T2, p.23).

Run 2022A: 13 Visits on schedule (Table T3, p.24). Plus the failed targets from 2021A to be scheduled.

Run 2022B: 12 Visits on schedule (Table T4, p.25). Plus the failed targets from 2021B to be scheduled.

5.3 Remote operation and data handling

All observations would be conducted remotely, either from Tucson, from Potsdam, or from the partner locations. The PEPSI User Interface is usually ported to LBT control room and is on stand-by once travelling is again possible and desired. Data will be stored in the standard PEPSI (SAN) data storage environment at LBTO and transferred to the PPIs once DR is complete and mature. Data transfer is via ftp/internet.

5.4 Data reduction and expected data volume

DR will be performed under the lead of Ilya Ilyin (AIP) with SDS4PEPSI on a larger computer. Final spectra are wavelength calibrated and continuum rectified and stored in FITS format. Each target or science case (c/o Sect. 2) has a PPI. The PPI is in charge of target logistics and its data product and is the lead author of the relevant publication. Additional deliverables from the same data product, e.g., a combined spectrum for host-star characterization, may be accessed by any Co-I in collaboration with the target PPI. The expected data volume is ≈2 TB. This poses no issue for PEPSI's SAN.

5.5 Bad weather rescheduling

As mentioned before, we expect losing about 50% of the scheduled transits/eclipses due to bad weather. "Bad weather" is defined as "dome closed for at least 30% of the transit duration" (including the ±1 hr pre- and post-transit observations). It thus marks also those transits/eclipses where bad weather allowed only partial time coverage, usually then with bad seeing, high winds and/or clouds accompanying, which definitely makes the science case unreachable. A target-by-target decision will be taken by the survey P.I. in collaboration with the PPIs. We ask that these targets will be rescheduled a year later in 2022 and 2023, respectively, based on a to-be-done science-merit ranking with respect to the regularly scheduled targets. The rescheduling shall then be based on these science merits once the failed targets are known. Therefore, such re-observations of the failed targets from the first semester 2021A may occur first time in semester 2022A which means that, on average, each of the semesters 2022A and 2022B will have 8 more targets than currently listed. Therefore, the current versions of Tables T3 and T4 are extended by these ghost targets as placeholders (colored in light red), while the time summaries in Table 2-4 already includes these targets by assuming average transit properties. Similarly, re-scheduling the targets that failed in 2022 to the two respective semesters in 2023 appears logic, but we note that it is currently a bit far into the future because of the unknown amount and prioritization of expected newly-discovered northern TESS targets. We plan to specify and request their compensation after a successful mid-term review but ask for the average 8 targets loss per semester already. Note that the science-merit ranking of the failed targets in 2021 will also take into account questions like, for example, was the science case successfully covered with another target?, or, had the PPI other successful transits and is busy with these data?, or had there been a publication on this target by another group in the meantime?, and there alike.

[1] V1298 Tau *bcd* have uncertain ephemeris by several hours. The planet discovery team (David et al. 2019, AJ **158**, 79) is working on a refinement that will be available for the first LBT scheduling for 2021B.

Table T1 – Target observing plan 2021A.

	Target	Transit Date (UT)	Eclipse Date (UT)	D (UT)	Host star char?	R	CD	PPI	Account
1	LTT3780b	Prio 1 4.03. Prio 2 5.02.	no	06:00-07:00 08:30-09:30	no	130	3+6	Molaverdikhani /Henning	LBTB/ MPIA
2	LTT3780b	Prio 1 14.03. Prio 2 12.02.	no	05:45-06:45 06:30-07:30	no	130	3+6	Molaverdikhani /Henning	LBTB/ MPIA
3	KELT-18b	Prio 1 21.04. Prio 2 1.04.	no	05:00 - 12:00 04:24 – 09:04	no	130	3+5	Keles	GTO
4	KELT-17b	Prio 1 4.02. Prio 2 10.03.	no	05:49 – 09:17 02:59 - 06:27	no	130	3+5	Keles	LBTB/AIP
5	HD80653b	Prio 1 14.02 Prio 2 27.02 Prio 3 4.02.	no	06:00 - 10:00 04:50 - 08:50 04:10 – 08:10	no	50	2+4	Yan/Henning	LBTB/ MPIA
6	HD80653b	Prio 1 9.02. Prio 2 22.02 Prio 3 12.03.	no	05:00 – 09:00 04:00 – 08:00 03:40 – 07:40	no	50	3+6	Yan/Henning	LBTB/ MPIA
7	HD80653b	no	Prio 1 18.02. Prio 2 5.02.	02:45 – 10:45 04:00 – 12:00	no	50	3+6	Yan/Henning	LBTB/ MPIA
8	WASP-12b	no	Prio 1 6.02. Prio 2 17.02 Prio 3 1.03.	5:52 3.00hr 3:49 3:57	no	130	3+5	Wang	OSURC
9	HD63433b	Prio 1 19.02. Prio 2 26.02.	no	03:11 – 08:23 05:10 - 10:22	no	250	3+5	Poppenhäger	GTO
10	HAT-P11	Prio 1 22.05.	no	06:00 – 10:30	yes	POL	3+5	Strassmeier	GTO
11	KELT-20b	no	Prio 1 15.06. Prio 2 22.06. Prio 3 29.06.	9:00 3.57hr 7:46 6:31	no	130	3+5	Wang	OSURC
12	KELT-9b	no	Prio 1 10.06. Prio 2 13.06. Prio 3 16.06.	9:00 3.92hr 8:06 7:11	no	130	3+5	Wang	OSURC
13	WASP-74b	Prio 1 12.07 Prio 2 27.06.	no	06:25 – 08:55 07:15 – 09:45	no	50	3+5	Shkolnik	AZ
14	WASP-13b	Prio 1 8.02. Prio 2 in 21B	no	04:15 – 10:15	yes	130	2+4	Sicilia	INAF
15	HD106315c	Prio 1 12.04. Prio 2 in 22A	no	02:40 – 09:30	yes	130	2+4	Sozzetti	INAF
16	Mascara-1b Phase 0.4	no	Prio 1 10.06. Prio 2 8.07.	07:11 - 11:07 05:21 - 09:42	yes	130	3+6	Scandariato	INAF
17	Mascara-1b Phase 0.6	no	Prio 1 19.06. Prio 2 4.07.	06:35 - 11:07 06:36 - 11:13	…	130	3+6	Scandariato	INAF

Notes: D Transit duration as UT range. R Resolution in 10^3. CD Cross Disperser. Two CD combinations mean alternating exposures in these two combinations. PPI Program Principal Investigator. Three visits on HD80653 (2x transit, 1x eclipse). Two visits on LTT3780. Host-star: "yes" means that one very good S/N spectrum in the remaining CDs will be taken.

Table T2 – Target observing plan 2021B.

	Target	Transit Date (UT)	Eclipse Date (UT)	D (UT)	Host star char?	R	CD	PPI	Account
1	TOI-1685	Prio 1 4.11. Prio 2 27.12.	no	07:15 – 10:00 04:15 – 07:00	no	130	2+4 & 3+6	Keles	GTO
2	V1298 Tau b	Prio 1 23.09. Prio 2 22.01.	no	09:00 – 15:25 01:45 – 08:10	yes	50	3+5/ 3+6	Poppenhäger Schlawin	GTO
3	V1298 Tau c	Prio 1 12.11. Prio 2 9.01.	no	07:22 – 12:01 01:17 – 05:57	no	50	3+5	Poppenhäger Schlawin	LBTB/AIP & GTO
4	V1298 Tau d	Prio 1 28.10. Prio 2 29.12.	no	04:55 – 10:30 05:18 – 10:53	no	50	3+5	Poppenhäger Schlawin	LBTB/AIP & GTO
5	WASP-82b	Prio 1 16.11. Prio 2 28.10. Prio 3 5.12	no	5:00 – 10:00 6:20 – 11:20 3:30 – 08:30	no	50	3+5	Shkolnik	AZ
6	HD189733b	Prio 1 11.09.	no	02:30-06:00	no	130	3+5	Mallonn	GTO
7	HD189733b	Prio 1 1.10.	no	01:45-05:15	no	130	3+5	Mallonn	GTO
8	WASP-76b	no	Prio1 10.09. Prio2 30.09. Prio3 29.10.	9:48 3.6936 7:36 6:36	no	130	3+5	Wang	OSURC
9	HAT-P-70b	Prio 1 27.12. Prio 2 16.12. Prio 3 5.12.	yes (2x)	03:30 – 07:00 04:00 – 07:30 04:40 – 08:10	no	50	3+5	Yan/Henning	LBTB/ MPIA
10	HAT-P-70b	no	Prio 1 9.12. Prio 2 20.12. Prio 3 31.12.	03:30 – 07:30 02:45 – 06:45 02:00 – 06:00	no	50	3+6	Yan/Henning	LBTB/ MPIA
11	HAT-P-70b	no	Prio 1 9.11. Prio 2 20.11. Prio 3 14.01.	06:30 – 10:30 06:00 – 10:00 03:15 – 07:15	no	50	3+6	Yan/Henning	LBTB/ MPIA
12	Mascara-1b	Prio 1 29.09. Prio 2 27.10.	no	03:11-07:14 01:39-05:42	no	130	3+5	Wang/Johnson	OSURC
13	HAT-P11	Prio 1 6.10.	no	02:30 – 07:00	yes	POL	3+5	Strassmeier	GTO
14	GJ892	Prio 1 2.11. Prio 2 5.10.	no	02:30 – 03:30 06:30 – 07:30	yes	130	2+4 3+6	Keles/Henning	GTO
15	KELT-17b	Prio 1 12.12. Prio 2 15.01.	no	07:15 – 12:45 04:30 – 10:00	no	130	SX2+4 &3+6 & MODS	Keles	GTO
16	HAT-P-47b	Prio 1 9.11. Prio 2 28.11,	no	05:12 - 10:18 03:30 – 08:36	yes	130	2+4	Pino	INAF
17	WASP-13b	Prio 1 27.12.	no	07:13 – 13:13	yes	130	3+6	Sicilia	INAF

Notes: Three visits on HAT-P-70 (1x transit, 2x eclipse). Three visits on V1298Tau, two visits on HD189733b.

Table T3 – Target observing plan 2022A.

	Target	Transit Date (UT)	Eclipse Date (UT)	D (UT)	Host star char?	R	CD	PPI	Account
1	KELT-20b	Prio 1 27.06. Prio 2 20.06.	no	05:50 – 09:20 07:00 – 10:30	no	50	3+5	Shkolnik	AZ
2	Kepler-13Ab	Prio 1 18.06. Prio 2 25.06.	no	04:00 - 09:00 05:00 - 10:00	no	50	3+5	Poppenhäger	LBTB/AIP
3	WASP-189b	no	Prio 1 29.05 Prio 2 9.06. Prio 3 7.04.	03:45 – 08:30 03:45 – 08:30 07:10 – 12:10	no	130	3+5 & 3+6	Patience	AZ
4	HD189733b	Prio 1 24.06 Prio 2 3.07.	no	08:08 – 10:08 05:07 – 07:07	no	130	2+4	Keles	GTO
5	KELT-9b	Prio 1 19.06.	no	06:10 – 11:10	no	50	3+5	Shkolnik	AZ
6	TrES-4b	Prio 1 29.05 Prio 2 30.06.	no	05:02 – 10:42 04:42 - 10:21	yes	130	2+4	Malavolta	INAF
7	HD106315c	Prio 1 26.04.	no	02:54 – 09:11	yes	130	3+6	Sozzetti	INAF
8	WASP-103b Phase 0.4	no	Prio 1 5.05. Prio 2 6.05. Prio 3 31.05.	09:06 – 11:04 07:19 – 09:18 07:04 – 09:02	yes	130	3+6	Borsa	INAF
9	WASP-103b Phase 0.6	no	Prio 1 8.05. Prio 2 3.06. Prio 3 29.06.	08:25 – 10:24 06:23 – 08:22 04:22 – 06:21	…	130	3+6	Borsa	INAF
10	KELT-19b	Prio 1 4.02.	no	04:15 – 08:55	no	130	3+5	Gaudi	OSURC
11	WASP-12b	no	Prio 1 11.02. Prio 2 23.02.	05:40 3.00hr 05:48	no	130	3+5	Wang	OSURC
12	KELT-20b	no	Prio 1 18.05. Prio 2 25.05.	08:44 1.3hr 07:29	no	130	3+5	Wang	OSURC
13	KELT-9b	no	Prio 1 6.07 Prio 2 9.07	09:24 3.92hr 08:30	no	130	3+5	Wang	OSURC
14									
15									
16									
17									
18									
19									
20									
21									

Notes: Red colored blocks are reserved for the bad-weather targets from 2021A.

Table T4 – Target observing plan 2022B.

	Target	Transit Date (UT)	Eclipse Date (UT)	D (UT)	Host star char?	R	CD	PPI	Account
1	WASP-33b	no	Prio 1 28.09 Prio 2 9.10. Prio 3 20.10.	8:51 2.977hr 8:20 7:50	no	130	3+5	Wang	OSURC
2	KELT-20b	Prio 1 8.09. Prio 2 15.09.	no	04:45 – 08:15 03:30 – 07:00	no	50	3+5	Shkolnik	AZ
3	KELT-9b	Prio 1 13.09. Prio 2 16.09.	no	04:20 – 08:21 03:30 – 07:30	no	50	3+5	Shkolnik	AZ
4	V1298 Tau c	Prio 1 13.12. Prio 2 15.1.	no	?	yes	50	3+5	Schlawin/ Poppenhäger	AZ
5	V1298 Tau d	Prio 1 11.12.	no	?	…	50	3+5	Schlawin/ Poppenhäger	AZ
6	V1298 Tau	Prio 1 12.12. Prio 2 14.12.	no	full night	yes	130	all	Strassmeier	GTO
7	TRAPPIST-1b	Prio 1 29.9. Prio 2 26.9.	no	04:30-05:30 04:00-05:00	no	50	3+6	Molaverdikhani /Henning	LBTB/ MPIA
8	TRAPPIST-1b	Prio 1 2.10. Prio 2 5.10.	no	05:00-06:00 04:30-05:30	no	50	3+6	Molaverdikhani /Henning	LBTB/ MPIA
9	HAT-P-47b	Prio 1 22.9.	no	06:36 – 11:41	yes	130	3+6	Pino	INAF
10	WASP-12b Phase 0.4	no	Prio 1 27.11. Prio 2 28.11. Prio 3 21.12.	07:00 – 09:24 09:10 – 11:35 07:15 – 09:39	yes	130	3+6	Nascimbeni	INAF
11	WASP-12b Phase 0.6	no	Prio 1 18.12. Prio 2 19.12. Prio 3 30.12.	06:05 – 08:32 08:16 – 10:43 06:13 – 08:39	…	130	3+6	Nascimbeni	INAF
12	WASP-76b	no	Prio 1 26.10 Prio 2 4.11.	06:03 3.7hr 07:14	no	130	3+5	Wang	OSURC
13	HAT-P1-b	Prio 1 8.10. Prio 2 17.10.	no	03:15 – 07.55 01:35 – 06:15	no	130	3+6	Keles	GTO
14	TOI-1685	Prio 1 22.12.	no	04:30 – 07.15	no	130	3+6	Keles	GTO
14									
14									
15									
16									
17									
18									
19									
20									

Notes: Red colored blocks are reserved for the bad-weather targets from 2021B. Position 6 on V1298 Tau is for host-star characterization only.

6. Survey organizational plan

6.1 LBTO-side

LBTO provides the telescope operator and schedules the observations. Only in one case does the survey require non-standard telescope operation (for the HAT-P1 visual binary in dual monocular mode). All other targets are standard point sources and require classical binocular mode. Note that the elevation limit for the AdSecs must be set to its lowest possible limit of 30° for all targets. No other preparations than the standard telescope collimation are required.

6.2 PEPSI-side

AIP provides PEPSI and operates the survey including data calibration and data reduction. The PEPSI P.I. is also the survey P.I.. PEPSI calibration includes standard flat fields, bias read outs, and Thorium-Argon exposures and/or also Fabry-Perot scans for all of the instrument modes requested. These data are taken automatically during daytime. The SDS4PEPSI pipeline reads those FITS files and generates master frames from individual frames closest in time. Generic PEPSI preparation includes chamber stability monitoring, blue and red CCD-dewar pumping, local area network verification, disk-space pre-allocation and directory logistics along with regular maintenance work.

6.3 Data rights

Data rights are granted to each PPI and will remain with the PPI for one year. The one year is counted from the date of the availability of the reduced data, set by the time when the reduced 1-D data are being written onto the PEPSI archive hard disk. After this period the data will be made public. If a publication takes place earlier than this then the data will be automatically public at the time of publication. Raw and reduced data will be archived at LBTO and may be downloaded by any PPI after the proprietary period. Reduced data can be shared by the PPI at any time.

6.4 Publication policy

Scientific publications are envisioned to take place per target. These are led by the PPIs identified in Tables T1-T4 in the role of Principal Authors. Each Principal Author adds his/her own collaborators as coauthors for their papers. For the first (and/or the most major) publication of a particular target the Principal Author also invites all other survey PPIs from Tables T1-T4 as co-authors. To be included in the co-author list, an invited PPI must confirm willingness to be a co-author. No response means no co-authorship. The PEPSI team members Strassmeier and Ilyin, and the LBTO director Veillet remain fixed co-authors on all first/major papers. The PETS P.I. will be the point of contact with the Principal Author, ensuring that all PETS co-authors receive manuscripts in a timely fashion and coordinating any internal discussions about the manuscripts. The PETS P.I. and/or the LBTO director will convey to the Principal Author any concerns by LBTO or by the PEPSI operations team regarding observatory policy in the best interests of the survey members.

We aim for a series of numbered papers in various journals under a joint main title and a roman lettering for the subtitle. The main title shall identify the survey. The subtitle shall be specific to the target in the paper. Although not final we envision the following:

The PEPSI-LBT exoplanet transit survey*

I. Water and potassium in HAT-P1-b

Footnote: *Based on data acquired with the Potsdam Echelle Polarimetric and Spectroscopic Instrument (PEPSI) using the Large Binocular Telescope (LBT) in Arizona.

Acknowledgements are the usual LBT add-ons: (1) via an asterisk at the survey title to the footnote with the text "*Based on data acquired with the Potsdam Echelle Polarimetric and Spectroscopic Instrument (PEPSI) using the Large Binocular Telescope (LBT) in Arizona.*" and (2) via adding the following text to the paper acknowledgement section: "*The LBT is an international collaboration among institutions in the United States, Italy and Germany. LBT Corporation partners are: The University of Arizona on behalf of the Arizona Board of Regents; Istituto Nazionale di Astrofisica, Italy; LBT Beteiligungsgesellschaft, Germany, representing the Max-Planck Society, The Leibniz Institute for Astrophysics Potsdam, and Heidelberg University; The Ohio State University, representing OSU, University of Notre Dame, University of Minnesota and University of Virginia.".*

For updates see https://www.lbto.org/ .

7. Project partners

The following list summarizes the project partners and their researchers involved in the survey. The parenthesis identifies the home institution and the red letter the LBT partner-time origin if not identical to the institution.

LBT partners:

Leibniz-Institute for Astrophysics Potsdam (AIP; account GTO or LBTB/AIP):

- Klaus G. Strassmeier, PEPSI Principal Investigator, survey P.I.;
- Ilya Ilyin, PEPSI instrument scientist, data reduction, and observer-in-chief;
- Katja Poppenhäger;
- Matthias Mallonn;
- Engin Keles;
- Xanthippi Alexoudi;
- David Gruner.

Large Binocular Telescope Observatory (LBTO):

- Christian Veillet, LBTO director, target scheduling, coordinating observational support.
- Olga Kuhn;
- Barry Rothberg;
- Michelle Edwards;
- Steve Ertel.

Italian National Institute for Astrophysics (INAF, account INAF):

- Daniela Sicilia;
- Luca Malavolta;
- Lorenzo Pino;
- Alessandro Sozzetti;
- Aldo Bonomo;
- Giusi Micela;
- Francesco Borsa;
- Isabella Pagano;
- Gaetano Scandariato;
- Laura Affer;
- Jesus Maldonado;

- Valentina D'Orazi;
- Valerio Nascimbeni;
- Laura Inno;
- Nicoletta Sanna;
- Anna Brucalassi;
- Giada Casali;
- Mauro Focardi;
- Laura Magrini;
- Monica Rainer;
- Germano Sacco;
- Maria Tsantaki;
- Mathieu Van Der Swaelmen;
- Katia Biazzo;
- Simone Antoniucci;
- Manuele Ettore Gangi.

University of Arizona (UoA; account AZ):

- Jennifer Patience;
- Chad Bender;
- Everett Schlawin;
- Thomas Beatty;
- Chenliang Huang.

Arizona State University (ASU; account AZ):

- Evgenya Shkolnik;
- Michael Line.

Ohio State University (OSU; account OSURC):

- Ji Wang;
- Scott Gaudi;
- Samson Johnson;
- Anusha J. Pai Asnodkar;
- Marc Pinsonneault.

Max-Planck-Institute for Astronomy (MPIA; account LBTB/MPIA):

- Thomas Henning;
- Fei Yan;
- Maria Bergemann;
- Laura Kreidberg;
- Paul Molliere.

Landessternwarte Heidelberg (LSW; account LBTB/MPIA)

- Karan Molaverdikhani;
- Sara Khalafinejad.

<u>Collaborators from LBT non-partners:</u>

University of Colorado, Boulder, U.S.A.:
- Wilson Cauley.

Las Cumbres Observatory, Goleta, U.S.A.
- Marshall C. Johnson

Wesleyan University, U.S.A.:
- Seth Redfield.

University of Nebraska at Kearne, U.S.A.:
- Adam Jensen.

Aahrus University Denmark:
- Carolina von Essen.

University of Bern, Switzerland:
- Daniel Kitzmann.

Space Research Institute Graz, Austria:
- Luca Fossati.

University of Tübingen, Germany:
- Rolf Kuiper.

Cornell University, U.S.A.:
- Jake D. Turner.

Grenoble-Alpes University, France:
- Aurelien Wyttenbach